Magnetotransport properties of arrays of cross-shaped antidots

S. de Haan and A. Lorke

Sektion Physik der LMU and Center for NanoScience, Geschwister-Scholl-Platz 1, D-80539 München, Germany

R. Hennig and M. Suhrke

Institut für Theoretische Physik, Universität Regensburg, D-93040 Regensburg, Germany

W. Wegscheider and M. Bichler

Walter-Schottky-Institut der TUM, D-85748 Garching, Germany

(Received 28 April 1999)

In magnetotransport measurements on arrays of cross-shaped antidots, we observe pronounced features in both the longitudinal and transverse magnetoresistivities ρ_{xx} and ρ_{xy}, which cannot be understood within the simple framework of commensurability between cyclotron radius and superlattice period. These resonances can be regarded as magnetotransport fingerprints of the complex unit cell. With the help of detailed numerical calculations using classical linear response theory we can ascribe additional maxima in ρ_{xx} to closed orbits in the dotlike potential between four antidots. A pronounced minimum in ρ_{xy} demonstrates the significance of open trajectories. [S0163-1829(99)13835-9]

I. INTRODUCTION

Two-dimensional electron gases (2DEG's) with a strong electrostatic modulation of the electron density, which is induced by periodic submicron voids, are called antidot arrays. The low-field magnetotransport properties of these systems are largely determined by the commensurability between the superlattice period a and the cyclotron radius R_c.[1–4] The longitudinal magnetoresistivity ρ_{xx} exhibits a series of maxima accompanied by nonquantized plateaus in the Hall resistivity ρ_{xy}. If the Fermi wavelength is sufficiently smaller than the superlattice period a, a classical theoretical approach taking into account the chaotic electron dynamics is feasible and has been proven successful to describe the dominant transport phenomena.[5] Assuming pinned classical cyclotron orbits in a billiard model of reflecting discs, each maximum in ρ_{xx} can be associated with commensurate trajectories encircling a certain number of antidots.

Additional features can be observed in the magnetoresistivity if the unit cell of the lattice becomes more complicated.[6–8] Here, we investigate an antidot array with such a complex unit cell, namely cross-shaped antidots. Due to its special structure this superlattice can also be regarded as an array of coupled quantum dots[9] or as an array of quantum point contacts (see inset of Fig. 1). It is therefore a promising candidate to study the transition between different types of quantization, e.g., between the quantized conductance in 1D channels at zero-magnetic field and the quantum Hall effect in 2D electron gases at high fields. The complex unit cell is reflected in the magnetotransport properties that we analyze with a classical approach. We find maxima in the longitudinal magnetoresistivity which can be ascribed to carrier trapping in the coupled dots. A pronounced quenching of the Hall resistivity can be understood in the picture of a series of point contacts.

The outline of the paper is as follows: In Sec. II, we describe the fabrication and the layout of our samples and the experimental techniques. Our numerical model is introduced in Sec. III, the experimental and numerical results are presented and compared in Sec. IV.

II. FABRICATION AND EXPERIMENTAL TECHNIQUES

The devices are fabricated from shallow GaAs/Al_xGa_{1-x}As heterostructures with a typical carrier density of 6×10^{11} cm^{-2} and a typical mobility of 8×10^5 cm^2/Vs at 4.2 K. High-resolution electron beam lithography and wet chemical-etching techniques are used to define a square array of antidots as part of a standard Hall bar geometry. A semi-
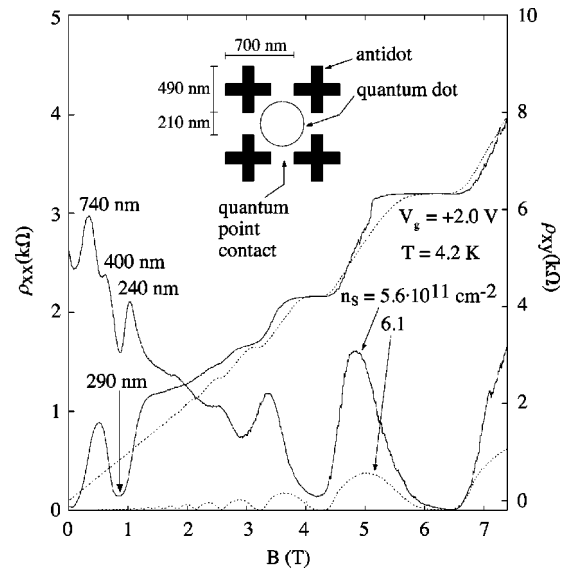

FIG. 1. Longitudinal and transverse magnetoresistivities of patterned (solid lines) and unpatterned (dotted lines) sample areas. Indicated in the main plot are the cyclotron diameters corresponding to the positions of the maxima. Inset: Sketch of the superlattice geometry.

transparent NiCr gate covering the entire central part of the Hall bar allows us to vary the electron density. We have chosen a lattice period of $a = 700$ nm (see inset of Fig. 1), which is much smaller than the electron mean-free path ($l_e \approx 10 \ \mu$m), but still much larger than the Fermi wavelength ($\lambda_F \approx 30$ nm). Various samples originating from different wafers have been fabricated this way and their longitudinal and transversal magnetoresistivities at liquid-helium temperature have been measured both before and after evaporating the gate electrode. Our Hall bar has four pairs of probes, enabling us to investigate the properties of the patterned and the unpatterned 2DEG on the same device and to compare the results directly.

III. NUMERICAL SIMULATIONS

As the Fermi wavelength λ_F for our electron densities is about 30 nm, and thus well below the size of the superlattice structure, we make use of classical transport theory to analyze the features in the magnetoresistivity, following the approach outlined in Ref. 5. Solving the classical equations of motion, we obtain a set of trajectories $x(t)$, $y(t)$ and velocities $v_x(t)$, $v_y(t)$. The antidots enter the equations of motion via a soft, two-dimensional model potential whose shape is sketched in the inset of Fig. 2(a). The potential height is adjusted such that the antidot size at the Fermi energy is in agreement with the lithographically defined structure.

This allows us to determine the conductivity tensor via linear response theory[10] by evaluating velocity-velocity correlation functions for a fixed Fermi energy. Scattering at ionized impurities, the dominant scattering process for the electrons at liquid-helium temperature, is considered by an exponential damping term with constant scattering time τ. The components of the conductivity tensor read

$$\sigma_{\mu\nu} = \frac{m^* e^2}{\pi \hbar^2} \int_0^\infty e^{-t/\tau} \langle v_\nu(0) v_\mu(t) \rangle_0 dt. \tag{1}$$

μ and ν refer to the directions x or y, m^* is the effective electron mass of GaAs and $\langle \ldots \rangle_0$ means an averaging over phase space at the Fermi energy.

IV. RESULTS AND DISCUSSION

In Fig. 1, we present a typical experimental result. The plot shows a comparison of the longitudinal and transverse magnetoresistivities obtained from the patterned and unpatterned areas of the sample. Due to depletion effects resulting from the Schottky gate, we have to apply positive gate voltages to make the device conducting. We would like to emphasize that this positive gate voltage does not affect the interpretation of the results, since the sample shows qualitatively the same behavior before fabricating the gate electrode [see solid lines in Figs. 2(b) and 2(c)]. As seen in Fig. 1, ρ_{xx} exhibits three clearly resolved maxima at low- and intermediate-magnetic fields. The Hall resistivity is quenched around $B = 0$ (Refs. 11 and 12) and exhibits a dramatic decrease well below the value of the unmodulated 2DEG around $B = 0.8$ T, where it drops almost to zero. At higher fields, ρ_{xy} exceeds the classical value and shows a behavior reminiscent of the ''last Hall plateau'' found in
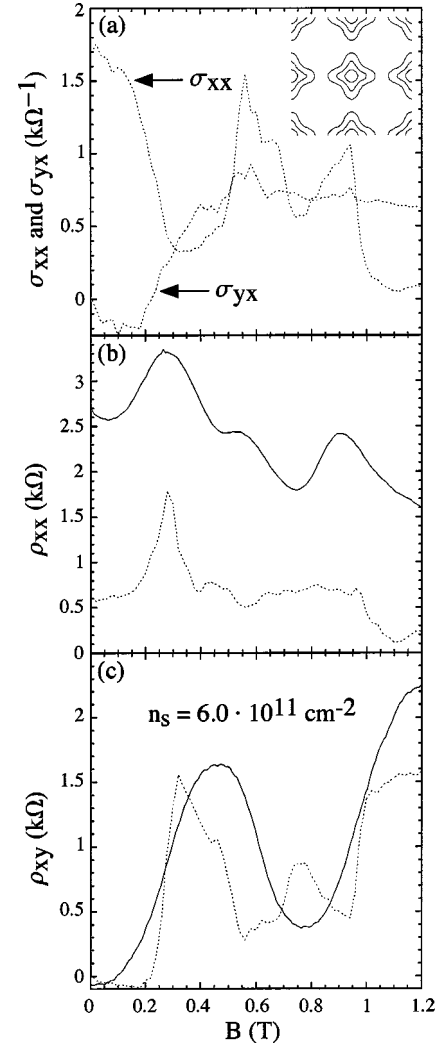

FIG. 2. (a) Longitudinal conductivity σ_{xx} and Hall conductivity σ_{yx} numerically calculated. Inset: Contour lines of the model potential used for the simulations. (b) and (c): Comparison of experimental (solid lines) and calculated (dotted lines) values of the longitudinal (b) and the Hall magnetoresistivities (c). Experimental data taken on an ungated sample.

ballistic cross junctions.[13,14] Finally, Shubnikov–de Haas oscillations accompanied by quantized Hall plateaus commence, and the traces from the patterned and unpatterned segments approach each other. This indicates that the intrinsic properties of the 2DEG are preserved in the regions between the antidots.

The classical cyclotron diameter $2R_c = 2(\hbar/eB)\sqrt{2\pi n_s}$ (cf. Fig. 1) is 740 nm at the dominant magnetoresistivity maximum, which is close to the lattice period. In contrast to results from arrays of round antidots,[2,3] characteristic features appear also at magnetic fields *above* this fundamental commensurability condition $2R_c = a$ at $B \approx 0.3$ T: two additional peaks in ρ_{xx} and the drastic decrease in ρ_{xy}. Commensurability maxima for lower magnetic fields cannot be resolved since trajectories enclosing a group of two or four antidots are not allowed for geometric reasons in a lattice of large antidots.[2] When varying the gate voltage and thus the electron density, only the maximum at $2R_c \approx a$ remains at a constant cyclotron diameter. The structures in the longitudinal and in the transverse magnetoresistivities at higher fields

shift both on the B and on the R_c scales. Taking into account that the gate is height-modulated, it becomes clear that a variation of V_g not only affects the electron density, but also strongly influences the effective size and shape of the antidots — the period on the other hand is fixed. So, from their position and the fact that they are very sensitive to the exact shape of the potential, we conclude that these new features reflect the complex structure of the basis rather than the superlattice period. However, they cannot easily be explained in terms of circular cyclotron motion within a hard-wall billiard model, as in our system the finite potential gradient between the antidots is not negligible.

To account for the additional structure we therefore perform numerical calculations for a soft model potential. The calculated longitudinal and transverse magnetoconductivities are plotted in Fig. 2(a). We obtain the corresponding resistivities by tensor inversion and compare them to the experimental data [cf. Figs. 2(b) and 2(c)]. Considering the complicated shape of the basis, the numerical results are in good agreement with our experiments. Even though no fit parameters were used in the calculations, we find not only qualitative similarity between experiment and simulation, but to a large extent even quantitative agreement. The experimental curves in Figs. 2(b) and 2(c) have been obtained from the same sample as the ones in Fig. 1, but before evaporating the NiCr gate. Compared to the measurements with gate, the observed structures are slightly shifted towards larger cyclotron diameters here. Different samples, however, show even quantitatively the same behavior, indicating that our observations are highly reproducible. Furthermore, similar features have been independently observed in ρ_{xx} by other authors.[8] The presence of the gate has a much stronger influence on the R_c values than, e.g., the wafer material used for fabrication. This fact shows again that the exact potential plays a more important role than in antidot lattices with a less-complicated basis. The first maximum in the longitudinal magnetoresistivity at $B \approx 0.3$ T, corresponding to the commensurability conditon $2R_c \approx a$ for round antidots, is very well reproduced by the simulation. This well-known peak is mainly caused by a minimum in the longitudinal conductivity that arises due to electrons encircling a single antidot. It is often accompanied by a shoulder in the Hall conductivity.[15] Here, the exact cyclotron diameter is $2R_c = 910$ nm, which is somewhat larger than the superlattice constant $a = 700$ nm. We ascribe this shift to soft wall effects in the electrostatic potential,[5] which influence the sensitive interplay between longitudinal and Hall conductivities. In our array of relatively large antidots compared to the lattice constant, these soft-wall effects lead to a deformation of the circular cyclotron orbits. Both the additional maxima in ρ_{xx} at the magnetic fields $B \approx 0.5$ and $B \approx 0.9$ T and the drop in the Hall resistivity, all of them above the fundamental commensurability condition, appear in the simulated curves as well. They are a unique feature of the cross-shaped antidot form.

To determine typical electron trajectories relevant for transport at a given magnetic field, we investigate the classical phase space by evaluating Poincaré sections. Due to the complex shape of the antidots the phase space structure is complicated and it is not always possible to attribute specific trajectories to each peak.
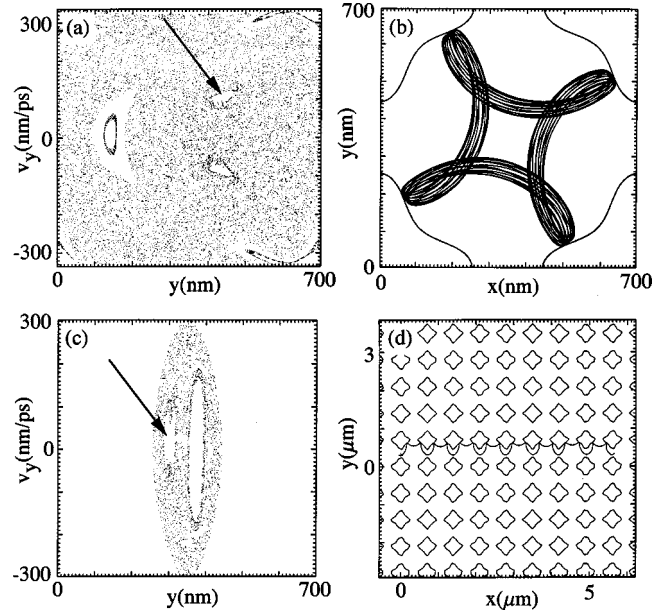

FIG. 3. (a) Poincaré section at the magnetic field of the second ρ_{xx}-maximum ($B \approx 0.5$ T) through the plane $x \bmod a = a/2$. (b) A typical trajectory, trapped in the quantum-dot-like potential between four cross-shaped antidots, with initial conditions located inside an island of stability [arrow in (a)]. The electrostatic potential is indicated by contour lines. (c) Poincaré section at the magnetic field of the σ_{xx}-maximum ($B = 0.55$ T) through the plane $x \bmod a = 0$. (d) "Runaway" trajectory with initial conditions of the left island of stability [arrow in (c)].

The Poincaré section in Fig. 3(a) for the maximum at $B \approx 0.5$ T shows three islands of stability near the center of the plot, each of them associated with electrons trapped in the potential minimum between four crosses. A typical trajectory is plotted in Fig. 3(b). Hence, the maxima in ρ_{xx} for higher magnetic fields reflect the fact that our superlattice can be regarded as a network of coupled quantum dots. Electrons are trapped for specific magnetic-field ranges within single dots reducing transport between neighboring unit cells.

In the following, we concentrate on the discussion of the minimum in ρ_{xy}, which is split into two minima in the simulation curve. The minima in the calculated ρ_{xy} curve clearly correspond to maxima in σ_{xx} [compare Figs. 2(a) and 2(c)]. Using the symmetry relations $\sigma_{xx} = \sigma_{yy}$ and $\sigma_{yx} = -\sigma_{xy}$ the transverse magnetoresistivity is

$$\rho_{xy} = \frac{\sigma_{yx}}{\sigma_{xx}^{\,2} + \sigma_{yx}^{\,2}}. \tag{2}$$

Considering that the Hall conductivity σ_{yx} depends only weakly on B for these magnetic fields and has the same order of magnitude as σ_{xx} [Fig. 2(a)], a maximum in σ_{xx} translates therefore approximately into a minimum in ρ_{xy}.

In order to understand the behavior of σ_{xx} we analyze the phase-space structure again. Figure 3(c) shows a Poincaré section for the σ_{xx}-maximum at $B = 0.55$ T with two islands of stability. The right one is associated with bound trajectories encircling one antidot and the left one with trajectories that channel along the principal axes of the lattice [see Fig. 3(d)].[15–17] Due to the concave shape of the walls in our system these so-called "runaway" trajectories are extremely

stable. According to the Kubo formula [Eq. (1)] such regular open trajectories translate directly into a high conductivity.

As in the experiments, the quantitative values for the calculated conductivities and resistivities depend sensitively on the exact shape of the potential and on the electron density, though the main features are qualitatively reproducible irrespective of the specific parameters. The double minimum of ρ_{xy} in the calculated data occurs for a carrier density of 6.0×10^{11} cm^{-2}. The open trajectories leading to the σ_{xx}-maximum at $B=0.95$ T differ slightly from the runaways at $B=0.55$ T. For higher and lower densities these different classes can no longer be resolved individually and the ρ_{xy} structure smears out to become one broad minimum similar to the experimental curve.

Open trajectories occur under the condition that the electrons can successively pass neighboring constrictions between the cross-shaped antidots. If, at sufficiently low-gate voltages, these constrictions approach the quantum limit they have to be regarded as a series of quantum point contacts with a small number of occupied 1D subbands.[18–20] Thus, the antidot array can also be considered as an array of quantum point contacts. Low-temperature measurements of an expected conductance quantization in this system are presently underway.

In conclusion, we have measured novel magnetoresistance features in an array of cross-shaped antidots. In addition to the well-known ρ_{xx} peak at the commensurability condition $2R_c=a$, the longitudinal magnetoresistivity shows two maxima for higher magnetic fields. With the help of numerical simulations, using classical linear response theory, we attribute them to trajectories trapped in the dotlike potential between four antidots. The Hall resistivity shows a distinct minimum, which is accompanied by a maximum in the longitudinal conductivity at the same magnetic field. This feature is particular to the present antidot shape and is caused by stable runaway trajectories which link the dotlike minima through the constrictions between the antidots.

[1] K. Ensslin and P. M. Petroff, Phys. Rev. B **41**, 12 307 (1990).

[2] D. Weiss, M. L. Roukes, A. Menschig, P. Grambow, K. von Klitzing, and G. Weimann, Phys. Rev. Lett. **66**, 2790 (1991).

[3] A. Lorke, J. P. Kotthaus, and K. Ploog, Phys. Rev. B **44**, 3447 (1991).

[4] G. M. Gusev, Z. D. Kvon, V. M. Kudryashov, L. V. Litvin, Yu. V. Nastaushev, V. T. Dolgopolov, and A. A. Shashkin, Pis'ma Zh. Éksp. Teor. Fiz. **54**, 369 (1991) [JETP Lett. **54**, 364 (1991)].

[5] R. Fleischmann, T. Geisel, and R. Ketzmerick, Phys. Rev. Lett. **68**, 1367 (1992).

[6] A. Lorke, S. Wimmer, B. Jager, J. P. Kotthaus, W. Wegscheider, and M. Bichler, Physica B **249-251**, 312 (1998).

[7] R. Kaiser, B. Irmer, M. Wendel, T. Schlösser, H. Lorenz, A. Lorke, K. Ensslin, J. P. Kotthaus, and A. Gossard, in *The Physics of Semiconductors*, edited by M. Scheffler and R. Zimmermann (World Scientific, Singapore, 1996), pp. 1501–1504.

[8] T. Azuma and T. Osada, Physica B **256-258**, 397 (1998).

[9] A. Lorke, J. P. Kotthaus, and K. Ploog, Phys. Rev. Lett. **64**, 2559 (1990).

[10] R. Kubo, J. Phys. Soc. Jpn. **12**, 570 (1957).

[11] M. L. Roukes, A. Scherer, S. J. Allen, Jr., H. G. Craighead, R. M. Ruthen, E. D. Beebe, and J. P. Harbison, Phys. Rev. Lett. **59**, 3011 (1987).

[12] R. Fleischmann, T. Geisel, and R. Ketzmerick, Europhys. Lett. **25**, 219 (1994).

[13] C. J. B. Ford, S. Washburn, M. Büttiker, C. M. Knoedler, and J. M. Hong, Phys. Rev. Lett. **62**, 2724 (1989).

[14] C. W. J. Beenakker and H. van Houten, Phys. Rev. Lett. **63**, 1857 (1989).

[15] R. Schuster, G. Ernst, K. Ensslin, M. Éntin, M. Holland, G. Böhm, and W. Klein, Phys. Rev. B **50**, 8090 (1994).

[16] É. M. Baskin, G. M. Gusev, Z. D. Kvon, A. G. Pogosov, and M. V. Éntin, Pis'ma Zh. Éksp. Teor. Fiz. **55**, 649 (1992) [JETP Lett. **55**, 678 (1992)].

[17] S. Lüthi, T. Vančura, K. Ensslin, R. Schuster, G. Böhm, and W. Klein, Phys. Rev. B **55**, 13 088 (1997).

[18] D. A. Wharam, T. J. Thornton, R. Newbury, M. Pepper, H. Ahmed, J. E. F. Frost, D. G. Hasko, D. C. Peacock, D. A. Ritchie, and G. A. C. Jones, J. Phys. C **21**, L209 (1988).

[19] D. A. Wharam, M. Pepper, H. Ahmed, J. E. F. Frost, D. G. Hasko, D. C. Peacock, D. A. Ritchie, and G. A. C. Jones, J. Phys. C **21**, L887 (1988).

[20] B. J. van Wees, H. van Houten, C. W. J. Beenakker, J. G. Williamson, L. P. Kouwenhoven, D. van der Marel, and C. T. Foxon, Phys. Rev. Lett. **60**, 848 (1988).